ScienSage

Journal of Advanced Scientific Research

Available online through https://sciensage.info

ISSN
0976-9595
Research Article

# INVESTIGATION OF SILICON-HYDRIDE NANODOTPROPERTIES USING DENSITY FUNCTIONAL THEORY

**Archana Kumari Singh, Satya Pal Singh*, Ankita Arya**

*Condensed Matter Physics &Nanoscience Laboratory, Department of Physics and Material Science,*
*Madan Mohan Malaviya University of Technology, Gorakhpur, Uttar Pradesh, India*
**Corresponding author: singh.satyapal@hotmail.com*

*Received: 05-07-2022; Accepted: 16-08-2022; Published: 31-08-2022*

 https://doi.org/10.55218/JASR.202213707

## ABSTRACT

The work aims to elucidate the optical and structural properties of silicon hydride nanoclusters and its bulk via density functional calculations. The molecular geometry is fully optimized with the help of DFT method using Gaussian 09 and Gaussian View 05 Software. Bandgaps are calculated using two approaches; first one using HOMO-LUMO concept and the second one is extracted from UV-vis spectrum. The calculated bandgap of silicon hydride is 3.7 eV. XRD data has also been analyzed using VESTA software, which shows the presence of a silicon matrix that contains organized silicon clusters forming an amorphous silicon matrix. A comprehensive investigation of amorphous films by X-ray diffraction (XRD) shows that the strongest peak in XRD patterns occurs at approximately 30.95°. Using XRD data, average size of optimized silicon hydride nano-cluster has been found to be 158.5 nm. Apparently large value of the cluster size can be attributed to the partially amorphous nature of silicon hydride nanocluster. The partial amorphous nature of silicon hydride is further confirmed from the analysis of its Raman spectrum. An overestimation of size in this case is not ruled out. Raman spectrum is calculated to further confirm deviations in nano-crystalline behavior. We also investigate and reveal properties using IR-spectrum, UV-vis-spectrum, NMR spectrum, and HOMO-LUMO gap.

**Keywords:** Silicon hydride Nanodot, DFT, XRD spectrum, Energy bandgap, HOMO-LUMO gap.

## 1. INTRODUCTION

Nanodots have wide range of applications in making sunscreens, military devices and equipment, electronic gadgets, photovoltaic cells and paintings and nano-scale drug delivery and therapeutic uses [1-4]. Semiconductor nanodots, also referred as quantum dots, because of the dominant role of quantum confinement effects, have recently attracted a great deal of attention because of their unusual and appreciable functional properties, stability. Nanostructures are materials with diameters less than 100 nanometers, which exhibit unique physical and chemical properties. Fabrication of such low-dimensional nanostructures, and their organization into hierarchical higher-order functional structures is expected to have crucial impact on future advances in science and industry. Controllable production of low-dimensional structures and the atomic- or molecular-level assembling of nanostructures into hierarchical structures has gained much attention in recent times.

The atomic structure of microcrystalline Si ($\mu$c-Si) comprises of Si organized domains with diamond crystal structure [5-11]. The diamond lattice is composed of two face-centered cubic (fcc) lattices that are separated by 1/4 of the diagonal length. Each Si atom is surrounded by four close neighbors, making a tetrahedron (the coordination number is 4). The unit cell of pure silicon lattice has 8 atoms, and the lattice constant is 5.4282 Å. Amorphous phase of Si has tetrahedral coordination bonds but with modest distortions in bond lengths and angles in comparison to its diamond crystalline phase. The distortions extend to only the first and second neighbors. In crystalline Si, the nearest distance between the two Si atoms is 2.35 Å (with a distortion of 1-3%), whereas the distance of a Si atom with the second neighbor is 3.5 Å (with distortions larger than 10 %). Si clusters of few nanometers in size, rather than tiny crystallites, are commonly used to describe ordered domains of Si. While it is well accepted that the diamond structure is not the most stable shape for small Si

clusters, there is no consensus on the structure of Si nano-crystallites. The slight amorphous nature of silicon hydride nanocluster has also been reported in ref nos. [12-15].

As simple hydrocarbons, silicon hydrides have boiling, melting, and dipole moment values comparable to simple hydrocarbons [12-15]. Both silicon hydrides and hydrocarbons exist in form of colorless gas or liquid at the room temperature. Hydrogenated silicon clusters have gained a lot of attention in the past decade due to its chemical structure and molecular bonding, as well as because of their vitality in modern industries. While homologous carbon and silicon entities are isovalent, their chemical characteristics can differ significantly. This is due to the fact that silicon has a larger p orbital than carbon, whereas carbon has a larger s orbital. On the other hand, hydrogenated silicon compounds play crucial roles in chemical vapor deposition of thin films, photoluminescence of porous silicon, potential surface fluctuations, and the Staebler-Wronski effect of hydrogenated amorphous silicon (a-Si:H); the effect refers to the light-induced changes e. g. increase in recombination current upon increase in light exposure reducing efficiency of a solar cell. This effect is important but poorly understood phenomenon. It is crucial to understand the equilibrium structures, thermo chemistry, and electron affinity of silicon hydride clusters in order to fully grasp these processes. As a result of this, we have used density functional theory to examine the electron affinities and their chemical structures in detail. Phases of silicon hydride and formed nanostructures are also discussed here in greater details in, parallel analogy with other studies [16-17].

The optical and electrical analysis of silicon hydride thin films deposited under varying applied conditions has been successfully carried out in order to understand the existence of definite crystalline and amorphous phases. The films had a relatively high band gap of 1.9 eV, as well as show significant photo response and dark conductivities of the order $10^5$ S/cm. The photo response of these nano-clusters opens up a wide range of applications for films, including thin-film transistors (TFT), anti-reflection coatings, and non-volatile memory devices, in addition to the photovoltaics. Furthermore, when a wide band gap thin film is used over another semi-conducting thin film with lower band-gap in making a photovoltaic cell, the photons having energies in between the band-gaps of the two layers, pass through the window layer and are absorbed by the lower film on the substrate to create electron-hole pairs at the depletion layer, whereas the photons having energies higher than the band-gap of the window layer, are adsorbed at the depletion layer sandwiched in between the two layers to form charge carriers [18-20]. Thus, the efficiency of the cell is greatly enhanced. This area has gained lot of attention in recent years.

## 2. METHODOLOGY

Density functional theory (DFT) is presently one of the most prevalent computational methods for the calculation of molecular electronic structure. The main advantage of this method is to calculate the energy of electronic system in form of electron probability density. Since electrons are tiny particles and follow laws of quantum mechanics, the material properties associated with them, must be characterized using quantum mechanical methods. In DFT calculations, electron density ($\rho$) rather than wave function ($\psi$), is used to calculate molecular structure. BP86 and B3LYP functionals are examples of GGA and hybrid functionals, respectively. This property of DFT allows to be used to model bond formation and bond-breaking processes, such as reaction mechanisms and kinetics to derive molecular scale characteristics [21-25].

Density functional approaches are mainly of three types. The methods of approximating local density (LDA) assume that the molecular density is uniform across the molecule, and is therefore not popular or practical in particular. The gas-chromatography (GC) approaches seek to determine the electron density non-uniformly. Hybrid methods, as its name suggest, are trying, with a number of enhancements to DFT Mathematics with combination of some of the most valuable elements of ab initio method (especially Hartree-Fock). The most often utilized approaches by computational chemistry practitioners are hybrid methods e.g. B3LYP. In contrast to *ab initio* approaches, the DFT methods may be employed for metal calculations as well. Some DFT techniques, including hybrid MPW1K approach, are specifically tailored for specific applications to solve kinetic problems. The remarkable advantage of DFT approach is that the accuracy has been significantly improved in its case, without further increasing computing time.

A set of functions (known as basis functions) which serve the purpose to combine and form linear super-position to express molecular orbitals, is the basis of theoretical and computational chemistry. To make it easier, such functions are often taken as atomic orbitals centered in

atoms but are subject to theory; plane waves are often utilized to construct such wave-functions. Here, we have used B3LYP functional with 3-21G basis set and have optimized the structure of silicon hydride using Gaussian 09 and Gauss View 05 software. As a semi-empirical basis set, the basis set 3-21G has been employed. Three primitives for the inner shells (STO-3G); each valence orbital is constructed using two sizes of basis function (two GTOs for representing contracted valence orbitals; one GTO for extended valence orbital). We use optimized structure's and perform XRD investigation using VESTA software. Fm-3m (225) space group is used to form it unit cubic cell structure [26].

## 3. RESULTS AND DISCUSSION

### 3.1. Optimized structure of Silicon Hydride Nanodot

We have created the structure of hydrogen bonded silicon atoms on Gauss view 0.5 software. Gauss 09 software is used to optimize the structure of hydrogenated silicon by DFT method and have obtained silicon hydride nanodot. The gray colored dots are used for Si atoms and the white color dots are used for hydrogen atoms. All the execution of programs end with imaginary frequency indicating for globally optimized structure of silicon hydride nanostructure as shown in Fig.1.

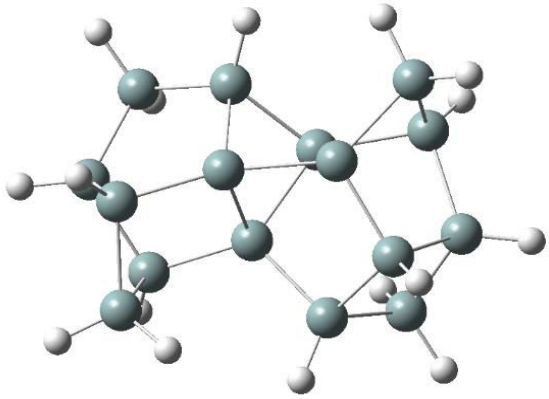

**Fig. 1: Nano structure of optimized Silicon hydride**

The data related with different properties of silicon hydride is provided in Table 1. 3-21G basis set has been used along with B3LYP functional. The silicon hydride nano-molecule bears zero charge. The molecule as a whole is neutral. Zero imaginary frequency ensures that the optimized structure is stable and in its ground energy state. Its Dipole moment is 0.212116 D and polarizability 462.532 a.u. This structure is optimized at temperature 298.150 K at 1 atm pressure using default setting of Gaussian 09. Thermal energy, heat capacity and entropy of silicon hydride are evaluated as 112.311 kcal/mol, 108.184 cal/mol-K, and 170.560 cal/mol-K, respectively.

### 3.2. Gaussian Calculation Summary

**Table 1: Summary of key properties of silicon hydride nanocluster**

| Property | Quantity | Unit |
|---|---|---|
| Imaginary Frequency | 0 | $cm^{-1}$ |
| Temperature | 298.1500 | Kelvin |
| Pressure | 1.0000 | atm |
| Dipole Moment | 0.2121 | Debye |
| Polarizability | 462.5320 | a.u. |
| Electronic Energy (EE) | -4617.3106 | Hartree |
| Zero-point Energy correction | 0.1515 | Hartree |
| Thermal Correction to Energy | 0.1790 | Hartree |
| Thermal Correction to Enthalpy | 0.1799 | Hartree |
| Thermal Correction to Free Energy | 0.0989 | Hartree |
| EE+Zero-point Energy | -4617.1591 | Hartree |
| EE + Thermal Energy Correction | -4617.1317 | Hartree |
| EE + Thermal Enthalpy Correction | -4617.1307 | Hartree |
| EE + Thermal Free Energy Correction | -4617.2117 | Hartree |
| Thermal Energy | 112.311 | kcal/mol |
| Heat Capacity | 108.184 | cal/mol-kelvin |
| Entropy | 170.560 | cal/mol-kelvin |

### 3.3. XRD Spectrum

In particular, X-ray diffraction (XRD) is used to determine the crystalline phase of a material, which can provide useful information about unit cell structure and its lattice parameters. In experimental procedures, after the material is homogenized, and finely powdered, XRD analysis is done for the average bulk composition. Identification of unknown crystalline materials is the most common application of X-ray diffraction (e. g. minerals, inorganic compounds). Unit cell of silicon hydride is shown in Fig. 2, obtained using Fm-3m space group in VESTA software. We have obtained XRD spectrum as shown in Fig. 3. This spectrum verifies the plasmonic state of silicon hydride nanoclusters. The highest intensity peak occurs due to the reflection through (1 1 1) plane at $2\theta = 30.9525°$ which is shown

in Fig. 3b. The second prominent peak is shown for the plane (2 0 0) at 35.8918° as shown in Fig. 3c. The reflection data for planes are given in Table 2. Using Scherrer formula, we calculated size of the nanocluster formed. The Scherrer formula is given by-

$$\tau = \frac{K\lambda}{\beta cos\theta} \quad (1)$$

Here, $\tau$ shows the average size of the nanoclusters formed, $K$ is shape factor with no dimension, having typical value 0.9, $\lambda$ shows the wavelength of X-ray used, $\beta$ is the line broadening of the peak at half intensity in radians, and $\theta$ is the Bragg's angle. Here, value of $\lambda$ is taken as 1.54432 Å, $\beta$calculated from graph for first prominent peak is 0.00091, and value of $\theta$ is 15.48°. The calculated average size of the formed silicon hydride nanocluster is 158.5 nm.

**Table 2: XRD data of silicon hydride nanocluster**

| No. | h | k | l | d (Å) | F(real) | F(imag) | \|F\| | 2θ | I | M | λ | Phase |
|---|---|---|---|---|---|---|---|---|---|---|---|---|
| 1 | 1 | 1 | 1 | 2.88675 | 4702.51 | 148.689 | 4704.86 | 30.9525 | 100.0000 | 8 | 1 | 1 |
| 2 | 1 | 1 | 1 | 2.88675 | 4702.79 | 149.342 | 4705.16 | 31.0293 | 49.7403 | 8 | 2 | 1 |
| 3 | 2 | 0 | 0 | 2.50000 | 4052.52 | 133.811 | 4054.72 | 35.8918 | 40.3920 | 6 | 1 | 1 |
| 4 | 2 | 0 | 0 | 2.50000 | 4052.76 | 134.399 | 4054.99 | 35.9817 | 20.0882 | 6 | 2 | 1 |
| 5 | 2 | 2 | 0 | 1.76777 | -1902.15 | -71.775 | 1903.5 | 51.6655 | 7.8661 | 12 | 1 | 1 |
| 6 | 2 | 2 | 0 | 1.76777 | -1902.28 | -72.0903 | 1903.64 | 51.7999 | 3.9105 | 12 | 2 | 1 |
| 7 | 3 | 1 | 1 | 1.50756 | -1790.94 | -72.9857 | 1792.42 | 61.4552 | 9.4232 | 24 | 1 | 1 |
| 8 | 3 | 1 | 1 | 1.50756 | -1791.07 | -73.3062 | 1792.57 | 61.6202 | 4.6844 | 24 | 2 | 1 |
| 9 | 2 | 2 | 2 | 1.44338 | -2039.56 | -82.9607 | 2041.25 | 64.5085 | 3.6625 | 8 | 1 | 1 |
| 10 | 2 | 2 | 2 | 1.44338 | -2039.72 | -83.325 | 2041.42 | 64.6837 | 1.8208 | 8 | 2 | 1 |
| 11 | 4 | 0 | 0 | 1.25000 | 62.671 | 3.73632 | 62.7822 | 76.0837 | 0.0019 | 6 | 1 | 1 |
| 12 | 4 | 0 | 0 | 1.25000 | 62.6779 | 3.75273 | 62.7901 | 76.3011 | 0.0009 | 6 | 2 | 1 |
| 13 | 3 | 3 | 1 | 1.14708 | 146.253 | 6.66359 | 146.405 | 84.3703 | 0.0347 | 24 | 1 | 1 |
| 14 | 3 | 3 | 1 | 1.14708 | 146.266 | 6.69285 | 146.419 | 84.6221 | 0.0173 | 24 | 2 | 1 |
| 15 | 4 | 2 | 0 | 1.11803 | 57.0505 | 3.13184 | 57.1364 | 87.0979 | 0.0051 | 24 | 1 | 1 |
| 16 | 4 | 2 | 0 | 1.11803 | 57.0564 | 3.14559 | 57.143 | 87.362 | 0.0025 | 24 | 2 | 1 |
| 17 | 4 | 2 | 2 | 1.02062 | -190.845 | -9.8059 | 191.097 | 98.0041 | 0.0534 | 24 | 1 | 1 |
| 18 | 4 | 2 | 2 | 1.02062 | -190.863 | -9.84896 | 191.117 | 98.3239 | 0.0267 | 24 | 2 | 1 |
| 19 | 3 | 3 | 3 | 0.96225 | 176.64 | 9.37952 | 176.889 | 106.359 | 0.0157 | 8 | 1 | 1 |
| 20 | 5 | 1 | 1 | 0.96225 | 268.782 | 14.2662 | 269.16 | 106.359 | 0.1091 | 24 | 1 | 1 |
| 21 | 3 | 3 | 3 | 0.96225 | 176.658 | 9.42072 | 176.909 | 106.73 | 0.0079 | 8 | 2 | 1 |
| 22 | 5 | 1 | 1 | 0.96225 | 268.808 | 14.3288 | 269.19 | 106.73 | 0.0547 | 24 | 2 | 1 |
| 23 | 4 | 4 | 0 | 0.88388 | 395.419 | 22.008 | 396.031 | 121.265 | 0.1432 | 12 | 1 | 1 |
| 24 | 4 | 4 | 0 | 0.88388 | 395.46 | 22.1047 | 396.077 | 121.76 | 0.0723 | 12 | 2 | 1 |

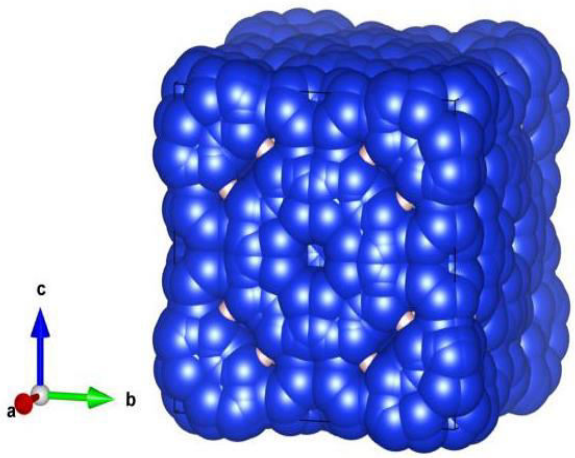


**Fig. 2: Unit cell of silicon hydride of dimension 5Å**

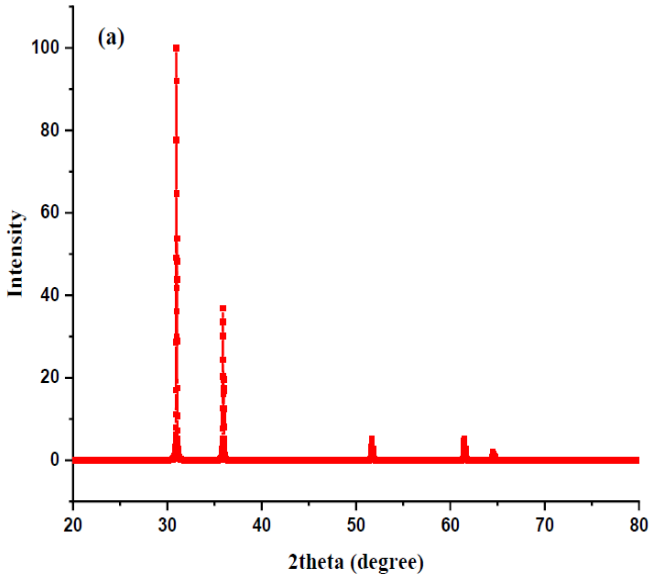

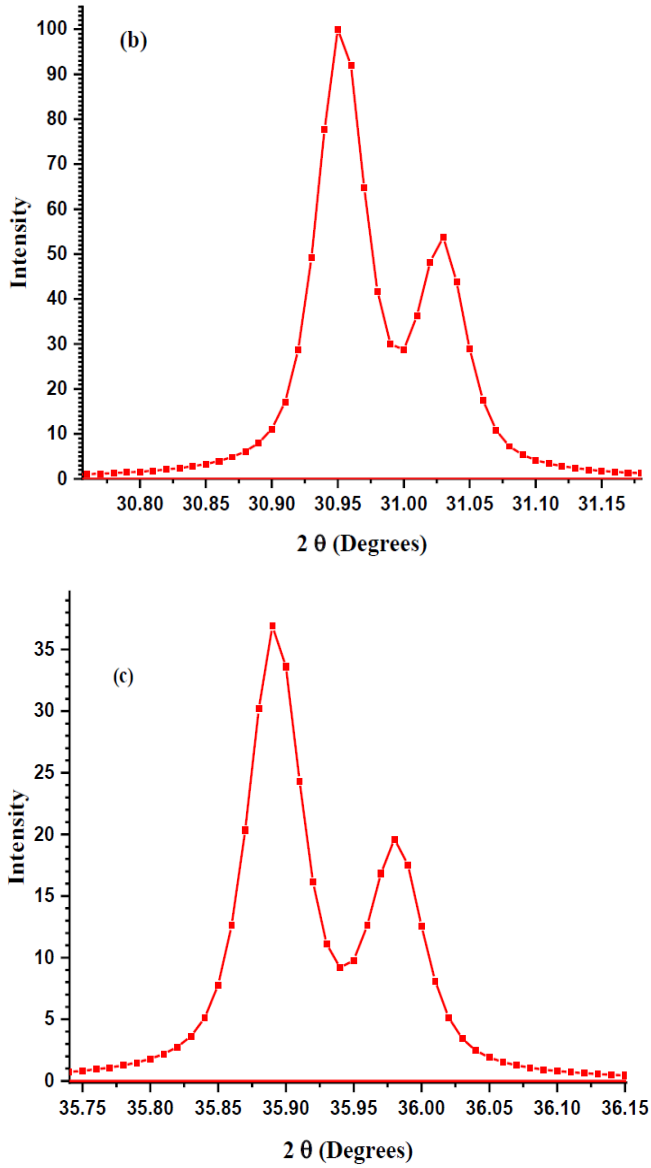


**Fig. 3: (a) XRD spectrum of silicon hydride (b) enlarged prominent peak-1 and (c) enlarged prominent peak-2 of silicon hydride nano-cluster.**

### 3.4. Raman Spectrum

Raman scattering is a sensitive method for analyzing Si:H materials, because it provides quantitative structural data related with the nanocrystalline and amorphous phases. Fig. 4 shows Raman spectrum of silicon hydride nanoclusters. Raman spectrum proves the near nano-crystalline nature of silicon hydride nanoclusters due to the prominent peak at the frequency 2174 $cm^{-1}$ formed because of Si-Si bond interactions as shown in Fig. 4a. Though, the strong peak near 2174 $cm^{-1}$ as shown in Fig. 4a appears to be sharp, but the original Raman graph Fig. 4c as obtained from Gaussian software reveals diffusive peaks indicating for deviation from perfect nano-crystalline phase towards amorphous phase. Similar diffusive peaks are also obtained below 900 $cm^{-1}$, which corresponds to the Si-H interactions. Thus, Raman plot further help us to confirm the XRD analysis.

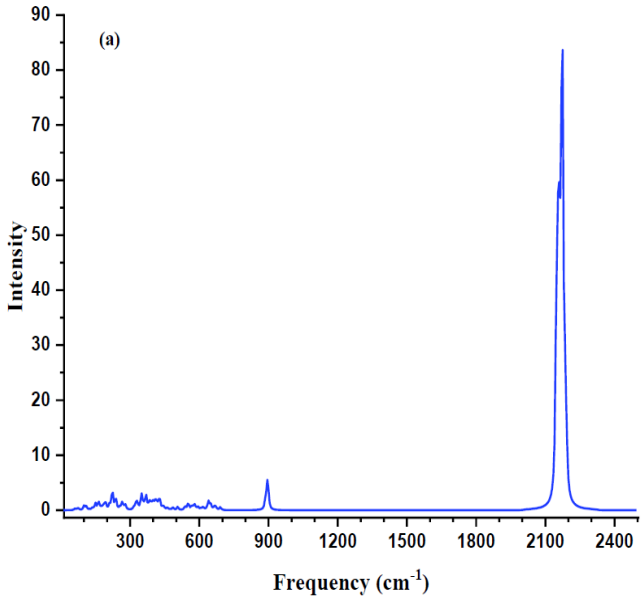


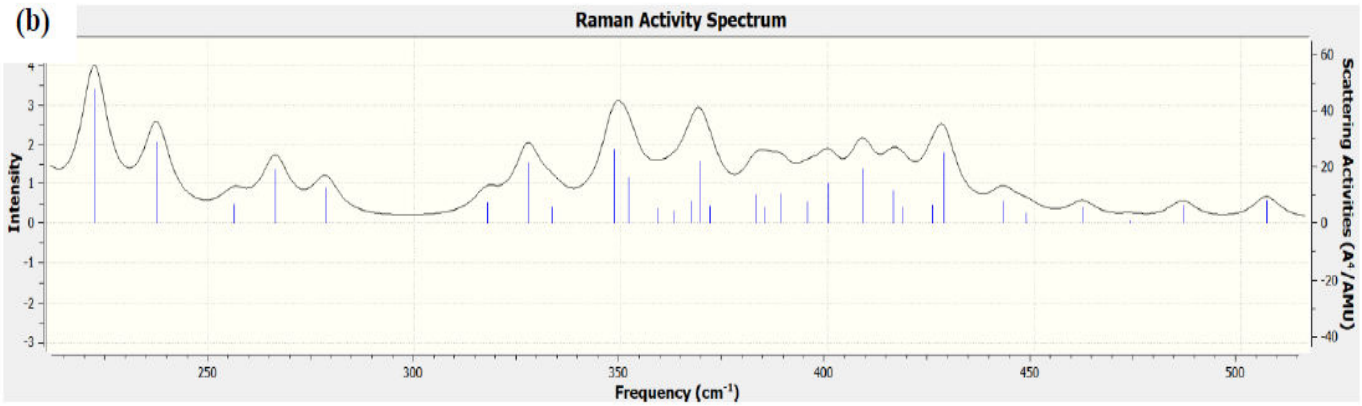

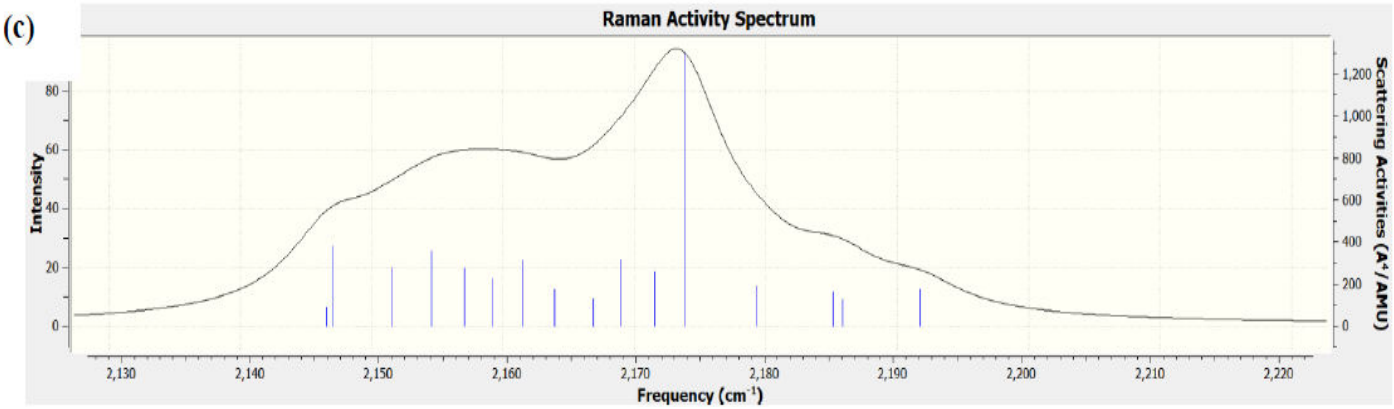


**Fig. 4: (a) Raman spectrum of silicon hydride nanocluster, (b) inset of the spectrum in far and mid infra-red region, and (c) inset of the spectrum in mid infra-red region**

### 3.5. IR Spectrum

IR spectrum is generated from molecule vibration states, which is the source of vital information. In addition to fundamental modes, there are also complex modes, vibrational overtones and summation modes of fundamental modes that are related to the vibrations of specific functional groups. For example, IR analysis can be used to determine the existence or absence of one or more fundamental modes of vibration in a material. It can be used to compare with an unknown spectrum existing in a database via using complicated pattern recognition algorithm or computer search-match algorithms.

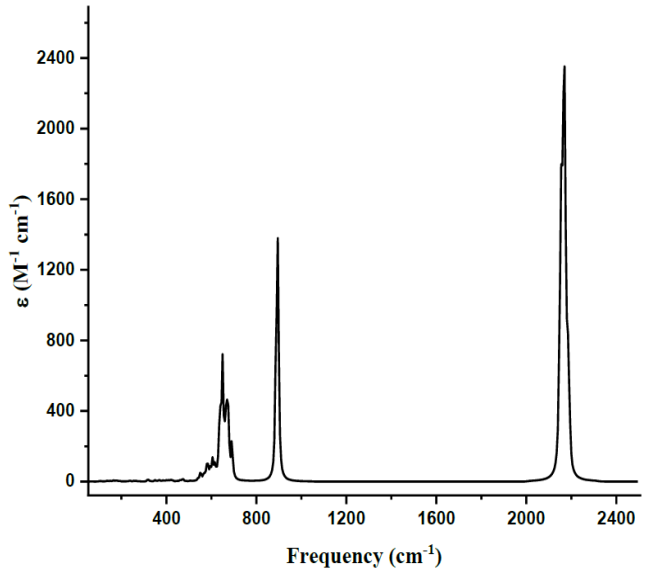


**Fig. 5: IR spectrum of Silicon Hydride**

The spectral data can also be utilized to measure one or more substances within a sample or complex mixture. IR spectrum of silicon hydride is shown in Fig. 5 in the frequency range 50 $cm^{-1}$-2500 $cm^{-1}$. The most prominent peak occurs at frequency 2171.4 $cm^{-1}$ due to 90$^{th}$ mode of vibration due to corner H-Si-H bond.

### 3.6. UV-Vis Spectrum

In semiconductor physics, UV-vis spectroscopy is used to determine the thickness and optical properties of thin layers on a slice. UV-vis signal is received for most of the molecules in the UV-vis region. Ultraviolet wavelengths range from 100-400 nanometers, while the visible light spectrum extends from 400 nm to 700 nm. Chemical substances absorb ultraviolet light or visible light, resulting in emission of visible spectra in UV-visible spectroscopy. Furthermore, the UV region has three linkages that encompasses the wavelength in the range of 100 nm-400 nm: UVA (315-400nm), UVB (280-315nm), and UVC (100-280nm). The wavelength of a reagent's intense photon absorption (the highest point along the spectrum's y-axis), the wavelength of maximum absorption (max), and the extent to which a material absorbs light, are all determined by the wavelength of light. The wavelength, at which a reagent exhibits maximum absorption, is abbreviated as $\lambda$max. It's also important to note that UV-vis spectroscopy shows a baseline at the bottom of the graph, with the edges at which peaks goes up and comes down. The graph shows, the highest peak of wavelength occurs at 450 nm as shown in Fig. 6. From UV-vis absorption spectrum first edge wavelength has been calculated as331.56 nm by drawing two tangent lines to the curve and dropping a vertical line at their intersection; the point above the vertical line at the curve has been used to draw unique tangent line giving precise band-gap

value as shown in Fig. 6b. This approach leads to indifferent values of band-gaps obtained by different authors as this scheme uniquely defines the point of inflexion [27]. Therefore, the bandgap is calculated by using the formula-

$$\Delta E = \frac{hc}{\lambda} = \frac{12400}{\lambda(A^o)} \text{ eV} \qquad (2)$$

Here edge wavelength $\lambda$ = 331.56 nm = 3315.6$A^o$
Therefore, bandgap = 3.74 eV ≈ 3.7 eV.

### 3.7. NMR Spectra

Chemical analysis using nuclear magnetic resonance (NMR), determines the quality and purity of samples as well as their molecular structures. NMR spectroscopy has been utilized in grade control and research for years. Many nuclei have a spin, and all nuclei are electrically charged, therefore if an outer magnetic field is applied, energy can be transferred resulting into a transition from low to a high energy state. It is possible to obtain NMR spectrum by adjusting or extending the magnetic field, while observing a single sample. The graph shows characteristic peaks indicating for the environment in which the hydrogen atom(s) are. The area under the peaks represents the numbers of hydrogen atoms in each of these settings, because it is proportional to the area under the peaks. The chemical shifts, gives us a lot of information about the environment in which the hydrogen atoms are there in. The NMR spectrum of silicon hydride nanocluster is shown in Fig. 7. The highest degeneracy is shown by four H atoms (i. e. 19-H, 21-H, 25-H, and 28-H) in the shielding range 28.0 ppm - 29.3 ppm.

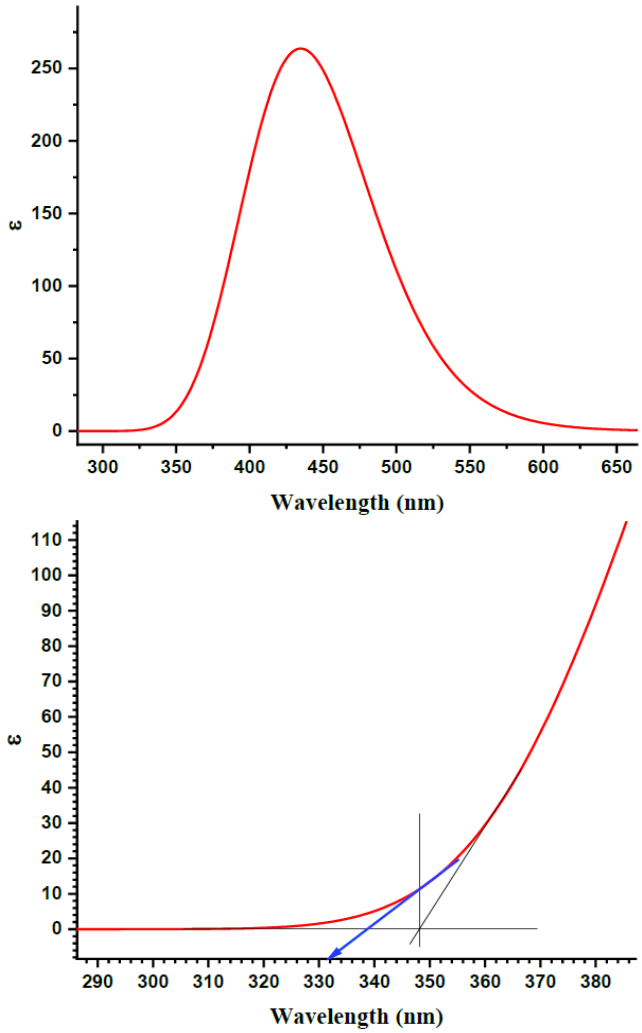


**Fig. 6: (a) UV-vis absorption spectrum and (b) edge wavelength of silicon hydride nanocluster.**

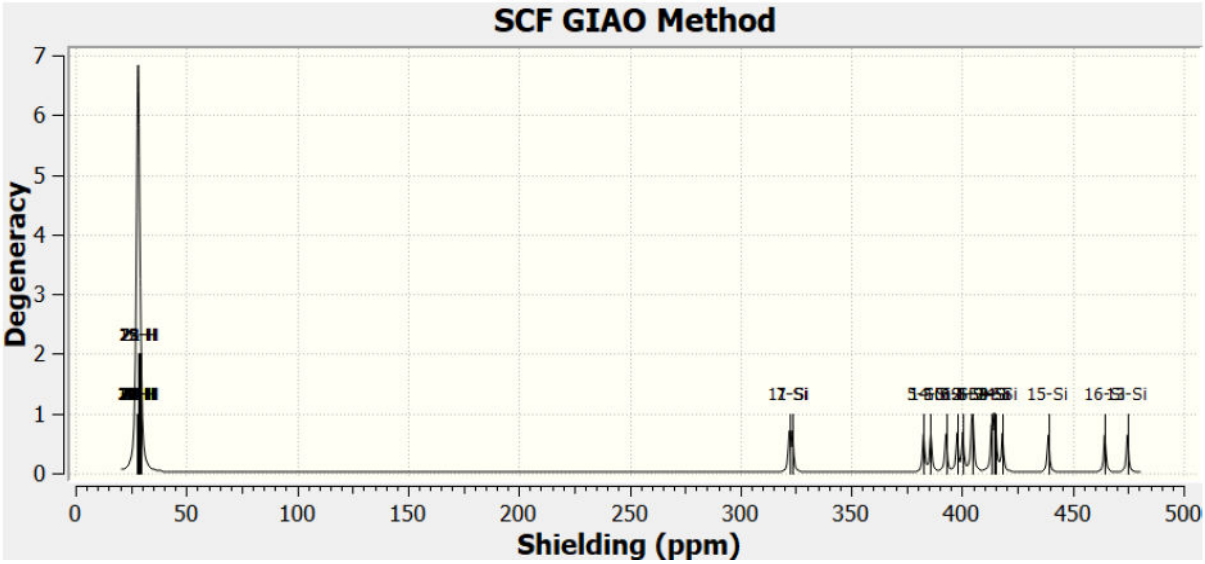


**Fig. 7: NMR spectrum of silicon hydride**

### 3.8. HOMO-LUMO of Silicon Hydride Nano-cluster

Molecular orbitals are divided into the highest occupied molecular orbital (HOMO) and the lowest unoccupied molecular orbital (LUMO) as shown in Fig. 8. An anti-bonding orbital can be created in the electronic state by adding energy to a molecule. An organic chemical reaction occurs, by making new bonds with other and/or dissociating from others. The HOMO-LUMO gap refers to the energy difference between the HOMO and LUMO states. Because of HOMO-LUMO transition, the electron goes into anti-bonding orbitals, resulting in an energetically instable state.

Orbitals of silicon hydride forms doublet, and thus splits into alpha- and beta- type molecular orbitals. First split molecular orbitals of silicon hydride nanocluster are shown in Fig. 9. The energy of the first alpha and beta LUMO orbitals are -0.08216 a. u. and of HOMO orbital is -0.21683 a. u. The energy bandgap calculated from LUMO-HOMO concept is 3.665 eV ≈ 3.7 eV, which is very close to the one obtained from UV-vis spectrum.

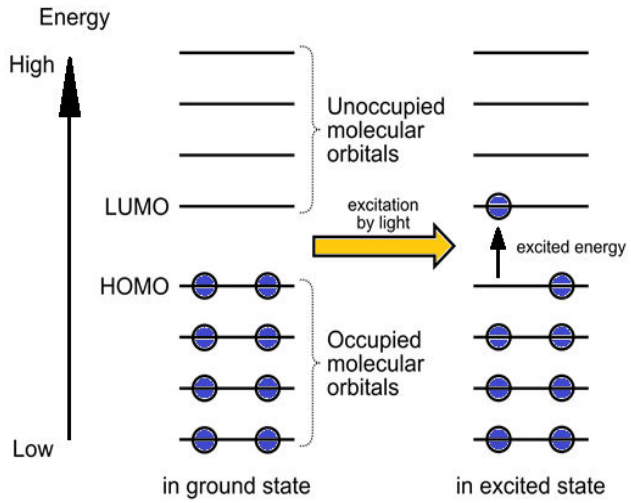


**Fig. 8: The energies of HOMO-LUMO of silicon vary with different electrical fields.**

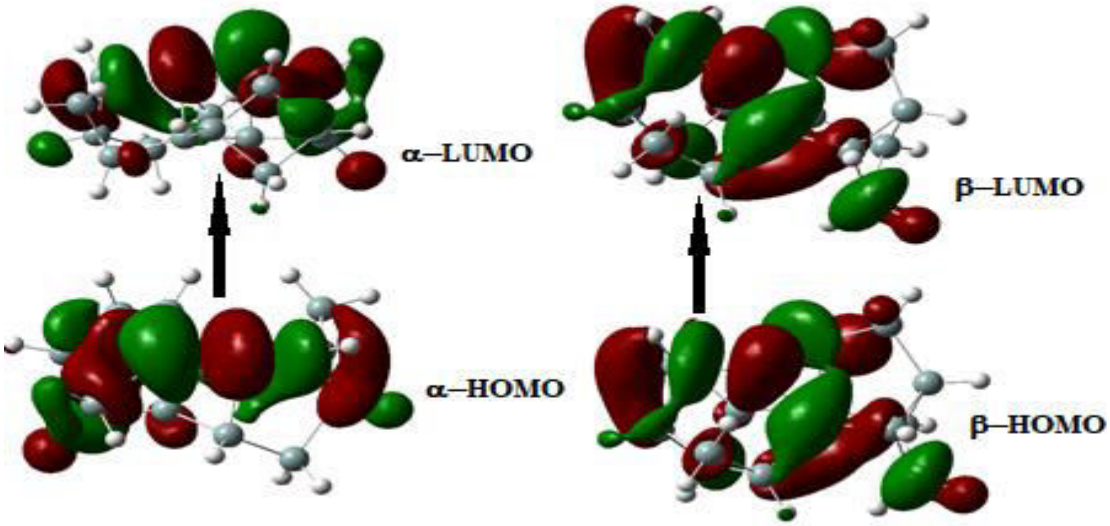


**Fig. 9: First HOMO-LUMO orbitals of silicon hydride nanocluster**

## 4. CONCLUSION

We have demonstrated that DFT-based calculations of silicon hydride nanocluster using Gaussian 09 software, successfully reveal vital information about the molecule along with producing its bulk properties. The methodology introduced in this work also serves the purpose of benchmarking for similar calculations. From XRD data, it has been shown that silicon hydride shows slight amorphous behavior, which has been further confirmed by Raman analysis.The calculated average size of nanocluster formed is 158.5 nm. IR, NMR, and UV-vis spectrum of silicon hydride nanocluster are calculated using DFT method. The bandgaps of optimized silicon hydride nanocluster calculated from both HOMO-LUMO gap and UV-vis spectrum are approximately 3.7 eV (wide band-gap) and are in very close agreements.

## 5. ACKNOWLEDGEMENTS

Authors are thankful to Prof. Umesh Yadav, Department of Physics, DDU Gorakhpur University,

Gorakhpur, UP, India-273009, for extending his support to the work.

***Conflict of interest***

None declared

## 6. REFERENCES


1. Guo D, Xie G, Luo J. *J. Phys. D: Appl. Phys,* 2014; **47**:13001.
2. Kolahalam LA, Viswanath IVK, Diwakar BS, Govindh B, Reddy V, Murthy YLN. *Mate. Tod. Procee*, 2019; doi.org/10.1016/j.matpr.2019.07.371
3. Rodriguez-Torres MDP, Pal K. In:Pal K. (eds) *Bio-manuf. Nanomate.* (Springer, Cham.)2021.
4. Ali A, Zafar H, Zia M, Haq I Ul, Phull AR, Ali JS, et.al. *Nanotech. Sci. Appl.*, 2016; **9**:49.
5. Shiohara A, Hanada S, Prabakar S, Fujioka K, Lim TH, Yamamoto K, et al. *J. Am. Chem. Soc.*, 2010; **132**:248.
6. Morozova S, Alkina M, Vinogradov A. *Front. Chem.*, 2019; **8**:191.
7. Cheng KY, Anthony R, Kortshagen UR, Holmes RJ, *Nano lett.*, 2011; **11**:1952.
8. Phan LMT, Baek SH, Nguyen TP, Park KY, Ha S, Rafique R, et al. *Mater. Sci. Eng. C*, 2018; **93**:429.
9. El-Atwani O, Ortoleva S, Cimaroli A, Allian JP. *Nanoscale Res Lett.*, 2011; **6:**403.
10. Peng K, Wang X, Lee S. *Appl. Phys. Lett,* 2009; **95**:243112.
11. Venugopal, Ren Z, Datta S, Lundstrom MS, Jovanovic DJ. *Appl. Phys.*, 2002; **92**:3730.
12. Linehan K, Doyle H. *J. Mater. Chem. C*, 2014; **2**:6025.
13. Li CP, Li XJ, Yang JC. *J. Phys. Chem. A*, 2006; **110**:12026.
14. Bertran E, Sharma SN, Viera G, Costa J, St'ahel P, Cabarrocas PR. *J. of Mater. Res.,* 1998; **13**:2476.
15. Waman VS, Funde AM, Kamble MM, Pramod MR, Hawaldar RR, Amalnerkar DP et al. *J. of Nanotech.*, 2011; doi:10.1155/2011/242398.
16. Kailer A, Gogotsi YG, Nickel KG. *J. Appl. phys.*, 1997; **81**:3057.
17. Cushing BL, Kolesnichenko VL, O'Connor CJ. *Chem. Rev.*, 2004; **104**:3893.
18. Chaudhary D, Sharma M, Sudhakar S, Kumar S. *Phys. Plasmas,* 2016; **23**:123704.
19. Cheng I C, Wagner S. *Devices and Systems*, 2003; **150**:339.
20. Nguyen HH, Nguyen VD, Trinh TT, Jang K, Baek K, Raja J, et al. *J Electrochem Soc*, 2011; **158**:H1077.
21. Shein M, Jeong WJ, Lee J. *J. Appl.Phys.,* 2016; **119**:154505.
22. Cohen AJ, Mori-Sánchez P, Yang W. *Science*, 2008; **321**:792.
23. Stoddart JC, March NH, *Annalas of Physics,* 1971; **64**(1):174.
24. Bédé AL, Assoma AB, Yapo KD, Koné MGR, Koné S, Koné M et al. *Comp. Chem.*, 2018; **06**(03):57.
25. Rocca D, Gebauer R, de Angelis F, Nazeeruddin MK, Baroni S. *Chem. Phys. Lett.*, 2009; **475**(1-3):49.
26. Viera G, Mikikian M, Bertran E, Cabarrocas PR, Boufendi L, *J. Appl. Phys*. 2002; **92**(8):4684.
27. Singh AK, Singh SP. *Liq. Crys.*, 2022; **49(5):**605-632.